Materials Science-Poland, 34(2), 2016, pp. 451-459
http://www.materialsscience.pwr.wroc.pl/
DOI: 10.1515/msp-2016-0059

DE GRUYTER OPEN

Effect of calcination temperature on the structural, optical and magnetic properties of pure and Fe-doped ZnO nanoparticles

RAMINDER PREET PAL SINGH[1], I.S. HUDIARA[2], SHASHI BHUSHAN RANA[3,*]

[1]Department of Electronics & Communication Engineering, Desh Bhagat University, Mandi Gobindgarh, India
[2]Chitkara University (Punjab Campus), Chandigarh, India
[3]Department of Electronics & Communication Engineering, GNDU Regional Campus, Gurdaspur, India

In the present study, pure ZnO and Fe-doped ZnO ($Zn_{0.97}Fe_{0.03}O$) nanoparticles were synthesized by simple co-precipitation method with zinc acetate, ferric nitrate and sodium hydroxide precursors. Pure ZnO and Fe-doped ZnO were further calcined at 450 °C, 600 °C and 750 °C for 2 h. The structural, morphological and optical properties of the samples were characterized by X-ray diffractometer (XRD), scanning electron microscope (SEM), energy dispersive spectroscopy (EDS) and UV-Vis absorption spectroscopy. The X-ray diffraction studies revealed that the as-synthesized pure and doped ZnO nanoparticles have hexagonal wurtzite structure. The average crystallite size was calculated using Debye-Scherrer's formula. The particle size was found to be in nano range and increased with an increase in calcination temperature. SEM micrographs confirmed the formation of spherical nanoparticles. Elemental compositions of various elements in pure and doped ZnO nanoparticles were determined by EDX spectroscopy. UV-Vis absorption spectra showed red shift (decrease in band gap) with increasing calcination temperature. Effect of calcination on the magnetic properties of Fe-doped ZnO sample was also studied using vibrating sample magnetometer (VSM). M-H curves at room temperature revealed that coercivity and remanent polarization increase with an increase in calcination temperature from 450 °C to 750 °C, whereas reverse effect was observed for magnetization saturation.

Keywords: *ZnO nanoparticles; co-precipitation; X-ray diffractometer; optical properties; UV-Vis absorption spectroscopy*

1. Introduction

ZnO is a group II – IV semiconductor that has become one of the most promising candidates for potential applications in optoelectronics due to its wide band-gap (3.3 eV) and high exciton binding energy (60 meV) properties [1, 2]. In order to optimize the structural, optical and magnetic properties of ZnO, a number of experiments have been done by various researchers either by using different capping agents or by doping ions into the ZnO lattice. Physical and chemical properties of zinc oxide vary with respect to the morphology of nanostructures. Therefore, not only various synthesis methods but also the physical and chemical properties of synthesized zinc oxide are to be studied with respect to its morphology [3].

Diluted magnetic semiconductors (DMS) have attracted much attention in recent years because they are the type of semiconductor in which fraction of host cations can be easily replaced by magnetic ions in fabrication of spintronics devices, such as spin valve transistor [4–7]. In the past few years, scientists have investigated the effect of ZnO nanoparticles doping with transition metals, such as Fe, Co, Ni and Mn [8–20]. Numerous theoretical explanations that have been proposed revealed that on doping ZnO nanoparticles with these transition elements results in dramatic changes in various luminescent and magnetic properties. These transition metals have been doped into the ZnO lattice to change the optical and magnetic properties,

---

[*] E-mail: shashi_rana12@yahoo.co.in

for the potential applications in spintronics devices, such as spin field effect transistor, gas sensor and quantum computers. In order to realize these objectives it is necessary to create ZnO based ferromagnetic materials, and understand their physical and structural properties. Experimental studies confirmed that the ferromagnetism strongly depends on synthesis technique and environmental conditions used for the preparation of the samples.

Most of the ZnO nanocrystals have been synthesized by traditional high temperature solid state reaction methods. However, these methods are time consuming and properties of the product cannot be controlled. ZnO nanoparticles can be prepared on a large scale at low cost by simple solution based methods, such as chemical co-precipitation, hydrothermal reaction, and sol-gel synthesis. In the present work, we have synthesized ZnO nanoparticles using co-precipitation method. This is a simple and low cost method that gives good yield of the end product and takes less time to prepare the nanoparticles. In this research work we have studied the effect of calcination temperature on the structural and optical properties of ZnO nanoparticles. Further, we have also studied the effect of calcination temperature on the structural, optical and magnetic properties of Fe-doped ZnO nanoparticles.

Organization of this research paper is summarized as follows: Section 1, illustrates the experimental procedure used to synthesize the ZnO nanoparticles, Section 2, describes the instrumentation used to characterize the structural, morphological and optical properties of ZnO samples. In Section 3, various results have been discussed in detail in terms of the nanoparticle properties, while the Section 4 concludes the paper.

2. Experimental

All the materials used in this work were of analytical reagent grade and were used without any further purification. In order to synthesize pure ZnO nanoparticles, zinc acetate ($Zn(CH_3COO)_2{\cdot}2H_2O$) was dissolved in distilled water and stirred for 1 hour. Aqueous solution of NaOH was added dropwise to the solution to maintain the pH ~ 10. The solution was then stirred at room temperature for 4 hours followed by aging for 24 h at the same temperature. After the aging, precipitate that formed was filtered and washed several times and was finally calcined at 450 °C, 600 °C and 750 °C for 2 h. Similarly, in order to synthesize the $Zn_{0.97}Fe_{0.03}O$ nanoparticles, the same steps have been followed, except adding ferric nitrate ($FeNO_3$), according to the calculated stoichiometric ratio.

2.1. Characterization of pure and doped samples

X-ray diffraction patterns of all the powder samples were recorded by a rotating angle X-ray diffractometer (Bruker AXS D8 Advance, Germany) equipped with a graphite monochromator and a mirror, at a fixed incidence angle of 1° to 5° and CuKα (wavelength = 1.540 Å, 40 kV, 100 mA) radiation source. The angular accuracy of the setup was 0.001° and the angular resolution was about 0.01°. The samples were scanned in an angular direction in the range of 20° to 90° (2θ) with the step size of 0.01°. Surface morphology of undoped (pure) and doped synthesized samples was determined by using scanning electron microscope Carl Zeiss Supras 55 which operated at a high acceleration voltage of 15 kV. The UV absorption spectra of the samples were recorded on the Systronics-2205 double beam spectrophotometer having a bandwidth of 1 nm and wavelength range of 200 nm to 1100 nm. Elemental composition of various samples was determined by EDS spectroscopy at an acceleration voltage of 200 keV. Magnetic hysteresis loop at room temperature was measured by using a vibrating sample magnetometer (VSM, Microsense EZ9) with a maximum magnetic field strength of 22.5 kOe.

3. Results and discussions

3.1. XRD analysis

Fig. 1 shows X-ray diffraction patterns of the synthesized pure ZnO samples calcined at different temperatures. Each XRD sample exhibits a hexagonal wurtzite phase. In all the samples peak intensity is very high which confirms good crystalline formation. It is clear from the XRD patterns that all the characteristic diffraction peaks can be indexed to the diffractions of (1 0 0), (0 0 2), (1 0 1), (1 0 2), (1 1 0), (1 0 3), (2 0 0), (1 1 2) and (2 0 1) planes with a hexagonal wurtzite structure. These diffraction peaks agree well with the values of the standard JCPDS No. 36-1451. XRD patterns clearly and show that the intensity of the peaks increases with an increase in calcination temperature, indicating increase in crystallinity at higher temperature.

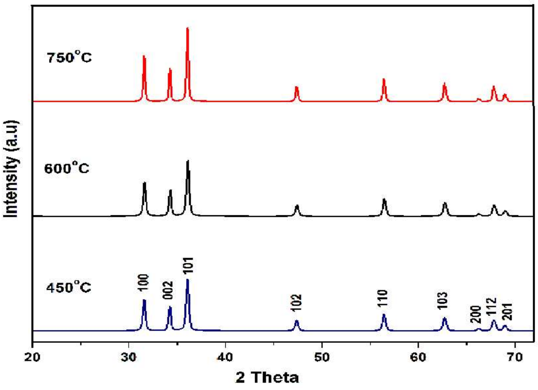

Fig. 1. XRD patterns of pure ZnO nanoparticles calcined at 450 °C, 600 °C and 750 °C.

The average crystallite size was calculated by using Scherrer's equation 1 and was found to be in the range of 31 nm to 42 nm as shown in Table 1:

$$\tau = \frac{k\lambda}{\beta\cos\theta} \tag{1}$$

where τ is grain size, β is the full width at half maximum, λ is the wavelength of X-ray (1.548 Å) and θ is the diffraction angle. From Table 1, it can be observed that the increase in particle size is significant at 750 °C as compared with the size at 600 °C. Migration of grain boundaries occurs at higher temperature which results in coalescence of small grains and forming large grains.

From the d-spacing values, lattice constants 'a' and 'c' were calculated using equation 2. The values are given in Table 1:

$$\frac{1}{d^2} = \frac{4}{3}\left(\frac{h^2+hk+k^2}{a^2}\right)+\frac{l^2}{c^2} \tag{2}$$

The calculated lattice parameters were also in good agreement with the values reported in literature.

Fig. 2 shows X-ray diffraction patterns of Fe-doped ZnO nanoparticles calcined at 450 °C, 600 °C and 750 °C. Each XRD sample exhibits the hexagonal wurtzite phase without any impurities and the secondary phase which shows incorporation of Fe dopant into the ZnO wurtzite lattice as a substitute atom. The intensity of the peaks in the XRD pattern is similar to that of pure ZnO, i.e. the peak intensity increases as the calcination temperature is increased. But, if we compare the corresponding peaks of pure and doped ZnO samples, it is observed that the intensity of doped samples decreases as compared to the pure samples. The further reveals that crystallinity reduces with the incorporation of Fe atoms into the ZnO lattice. It has been reported in literature that when a foreign particle is incorporated in a crystal lattice, it produces a strain as well as defects in the lattice which may deteriorate the crystal quality [21]. Table 2 summarizes the calculated average particle size and unit cell parameters. Average particle size varies from 29 nm to 38 nm. Again the variation is similar to that in the pure ZnO nanoparticles but the only difference is that the particle size decreases for the doped samples as compared to the pure samples at corresponding temperatures. The reason for that is due to introduction of large amount of foreign particles into the crystal lattice causing strain within the lattice and leading to lattice distortion, which results in a decrease in crystallinity of the material.

The ionic radii of Fe^{2+} and Fe^{3+} are different from that of Zn^{2+}. The ionic radii of Fe^{2+}, Fe^{3+} and Zn^{2+} are 0.078 nm, 0.068 nm and 0.074 nm, respectively. If Fe ions exist in ZnO mainly in the form of Fe^{2+}, due to larger ionic radius of Fe^{2+} ion than that of Zn^{2+}, it will lead to compression strain and, as a result, particle size increases [22]. On the other hand, if Fe ions exist in ZnO mainly in the form of Fe^{3+}, due to smaller ionic radius of Fe^{3+} ion than that of Zn^{2+}, it will lead to tensile strain and, as a result, particle size decreases [23]. Therefore, it is reported that Fe^{2+} and Fe^{3+} ions

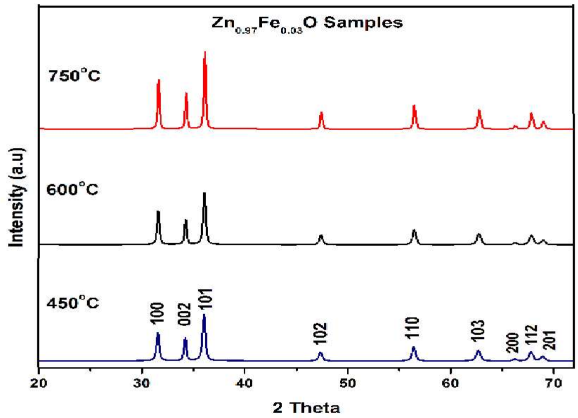

Fig. 2. XRD patterns of $Zn_{0.97}Fe_{0.03}O$ nanoparticles calcined at 450 °C, 600 °C and 750 °C.

may coexist which requires further investigation. For maintaining charge neutrality and to substitute Zn^{2+} ionic sites, the valence of Fe ion should be +2. The ionic radius of Fe^{2+} is larger than that of Zn^{2+} whereas that of Fe^{3+} is smaller. Therefore, it can be inferred that Fe^{2+} and Fe^{3+} ions coexist and are expected to distort the lattice structure for holding charge neutrality. So, in order to incorporate the Fe ions, crystal lattice of ZnO contracts or expands depending on the nature of the ion. So, all these factors lead to distortion or strain in the material and also produce defects which in turn affect the properties of the material.

Table 1. Lattice parameters of pure ZnO nanoparticles calcined at 450 °C, 600 °C and 750 °C.

Calcination temperature [°C]	Crystallite size D [nm]	d_{101} [λ]	Lattice constant a [Å]	c [Å]
450	31 nm	2.4874	3.247	5.303
600	33 nm	2.4854	3.244	5.299
750	42 nm	2.4881	3.248	5.304

3.2. Scanning electron microscopy (SEM) analysis

The morphology of pure and Fe-doped samples was observed by using a scanning electron microscope (SEM). Fig. 3 shows SEM images of pure ZnO nanoparticles calcined at 450 °C, 600 °C and 750 °C, respectively. The SEM images confirm that all the samples are in nano range which is in good agreement with the particle size calculation using the XRD technique. It is clearly seen that the particles are spherical in shape. Further, it is clear that the particle size goes on increasing with an increase in calcination temperature.

Table 2. Lattice parameters of $Zn_{0.97}Fe_{0.03}O$ nanoparticles calcined at 450 °C, 600 °C and 750 °C.

Calcination temperature [°C]	Crystallite size D [nm]	d_{101} [λ]	Lattice constant a [Å]	c [Å]
450	29 nm	2.4887	3.248	5.305
600	32 nm	2.4861	3.245	5.300
750	38 nm	2.4834	3.241	5.294

Similarly, Fig. 4 shows SEM images of Fe-doped ZnO nanoparticles calcined at 450 °C, 600 °C and 750 °C, respectively. All the samples are composed of particles in nano range which are spherical in shape as clearly seen from the SEM images. Further, it is clear that the particle size goes on increasing with an increase in calcination temperature. Comparing Fig. 3 and Fig. 4, the difference in particle size is clearly visible and again in good agreement with the XRD calculations.

Fig. 5 shows energy dispersive X-ray spectra (EDS) of pure and Fe-doped ZnO nanoparticles which confirm the elemental composition of the synthesized nanoparticles (undoped and doped). The EDS analysis confirms the presence of Zn, O and Fe in the doped sample with no other impurity element.

Fig. 5a to Fig. 5c show the EDS spectra of pure ZnO samples calcined at 450 °C, 600 °C and 750 °C, respectively. The EDS spectra indicate that the synthesized pure ZnO sample mainly contains Zn and O elements. The EDS spectral peak of O appears at 0.5 keV whereas Zn appears at 1 keV, 8.6 keV and 9.5 keV in all three samples. Fig. 5d shows the EDS spectrum of Fe-doped ZnO sample calcined at 600 °C. The EDS spectrum indicates that the synthesized Fe-doped sample mainly contains Fe, Zn, and O elements. The EDS spectral peak of O appears at 0.5 keV, Zn appears at 1 keV, 8.6 keV and 9.5 keV, while Fe signal appears at 0.7 keV, 6.4 keV and 7.2 keV.

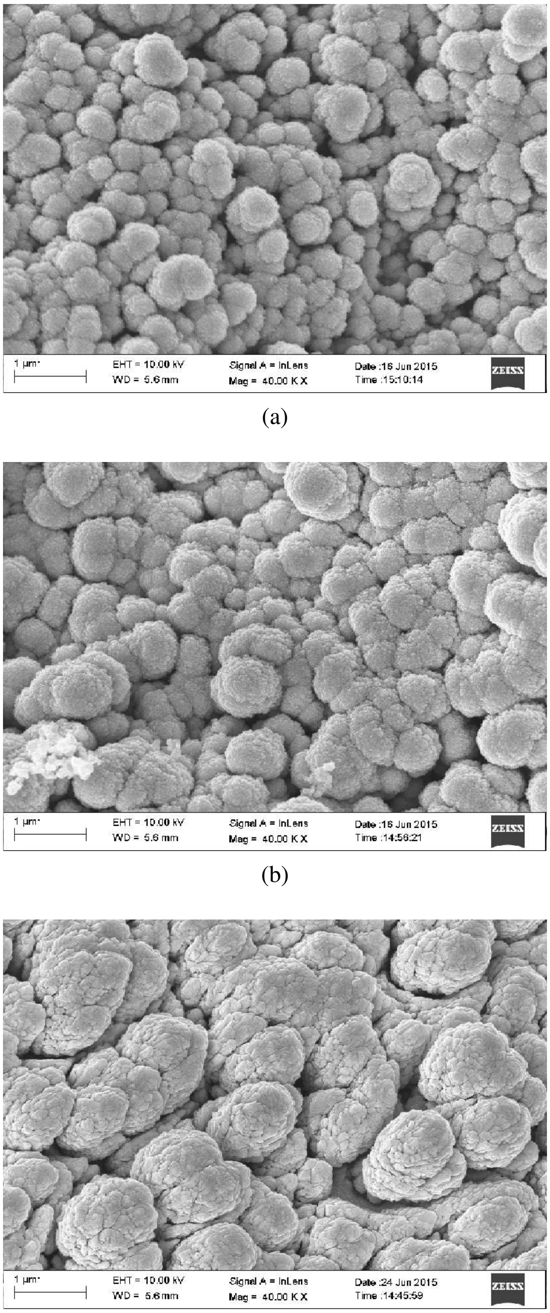

(a)

(b)

(c)

Fig. 3. SEM images of pure ZnO nanoparticles calcined at (a) 450 °C, (b) 600 °C and (c) 750 °C.

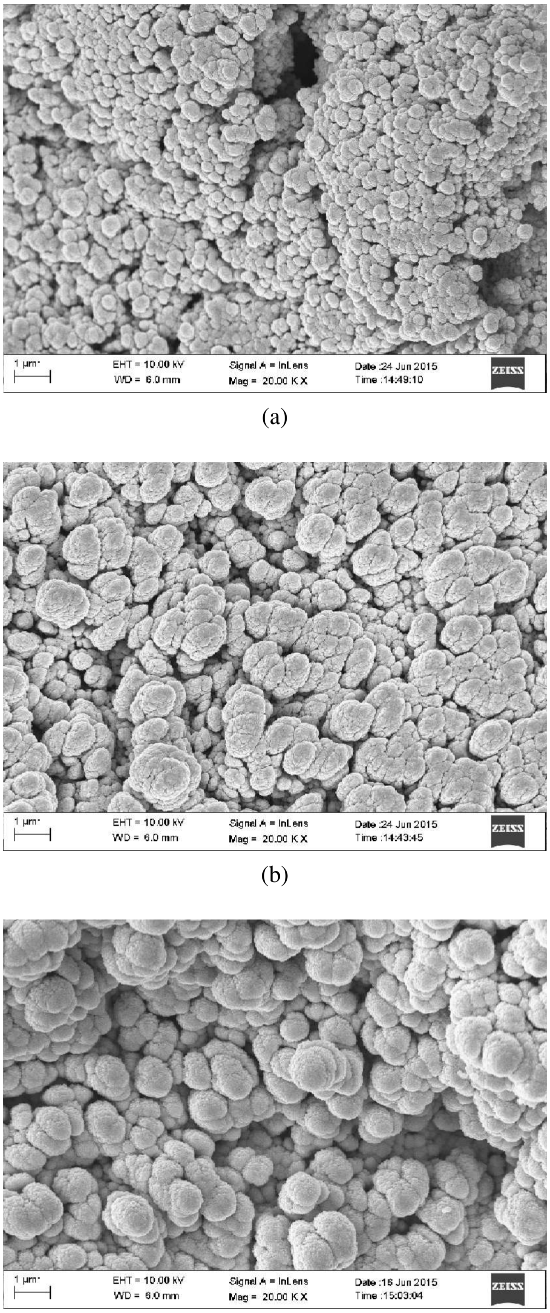

(a)

(b)

(c)

Fig. 4. SEM images of Fe-doped ZnO nanoparticles calcined (a) 450 °C, (b) 600 °C and (c) 750 °C.

The Zn ions concentration (wt.%) was found to be approximately 92.01 %, 91.69 % and 91.51 % for samples calcined at 450 °C, 600 °C and 750 °C, respectively, in pure ZnO samples as highlighted in Table 3. Fe ions concentration was found to be 2.18 % for Fe-doped samples calcined at 600 °C. The EDS results further verify the XRD results, which reveal that Fe-doped ZnO diluted magnetic semiconductor was successfully synthesized by the chemical precipitation method.

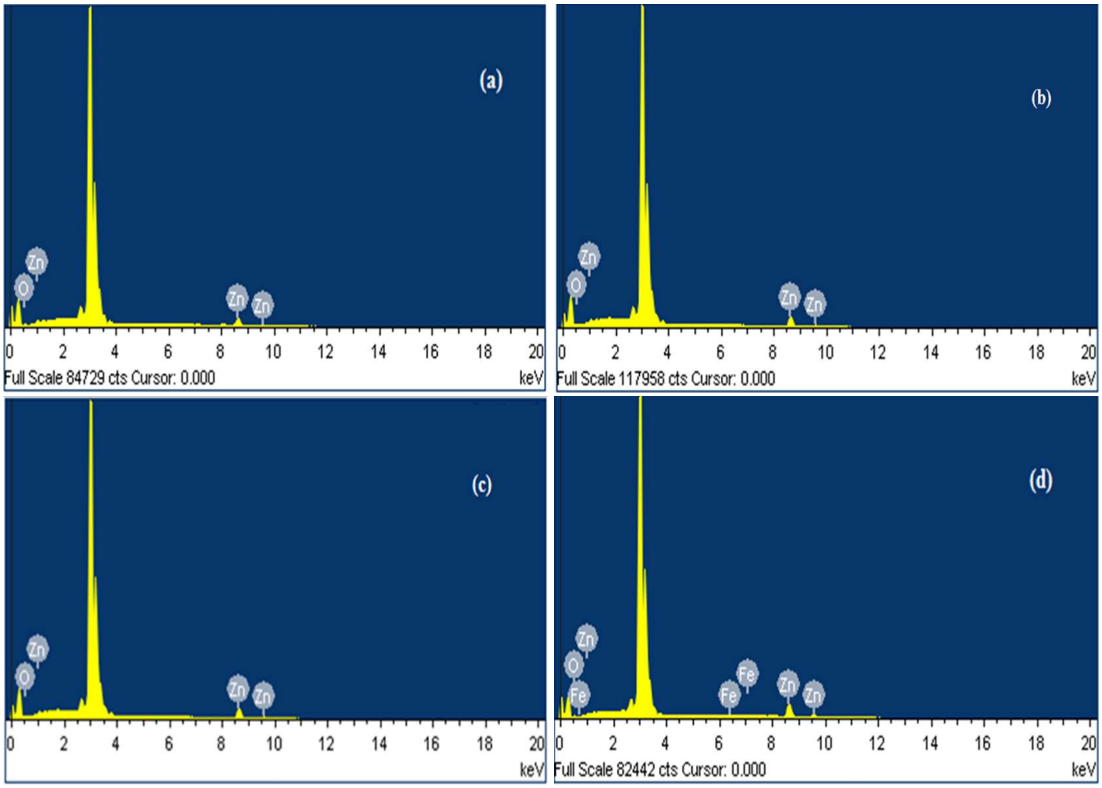

Fig. 5. X-ray energy dispersive spectrometry (EDS) spectra of (a-c) pure ZnO sample calcined at 450 °C, 600 °C and 750 °C and (d) $Zn_{0.97}Fe_{0.03}O$ sample calcined at 600 °C.

Table 3. EDAX data of pure ZnO nanoparticles.

Calcination temperature [°C]	Zn [%]	O [%]
450	92.01	7.99
600	91.69	8.31
750	91.51	8.49

3.3. Optical absorption study

Results for pure and doped ZnO nanoparticles were compared by using the UV-Vis absorption spectroscopy. The band gap of semiconductor nanoparticles changes with a change in particle size. The UV-Vis absorption study of pure and Fe-doped ZnO nanoparticles samples has been carried out over the wavelength range of 300 nm to 800 nm. Fig. 6a shows the absorption spectra of the pure ZnO nanoparticles with the absorption peaks at 388 nm, 392 nm and 398 nm for calcination temperatures of 450 °C, 600 °C and 750 °C, respectively. Similarly, Fig. 6b shows the absorption spectra of the Fe-doped ZnO nanoparticles with the absorption peaks at 384 nm, 389 nm, and 395 nm for calcination temperatures of 450 °C, 600 °C and 750 °C, respectively.

The value of the absorbance is dependent on the various factors, such as size of particles, flaws or defects in grain structure and oxygen deficiency. Lower band gap value (Eg) of pure and doped ZnO sample compared to bulk ZnO (3.39 eV) might be due to the presence of oxygen vacancy defects, which is in good agreement with the Eg value determined in the literature [24, 25]. From Table 4 and Table 5, it is seen that the band gap energy decreases with the increase in calcination temperature due to the increase in the particle size as has also been evident from the XRD results.

In contrast to pure ZnO, an increase in the value of band gap energy in doped ZnO nanoparticles is due to the sp-d spin exchange interaction between

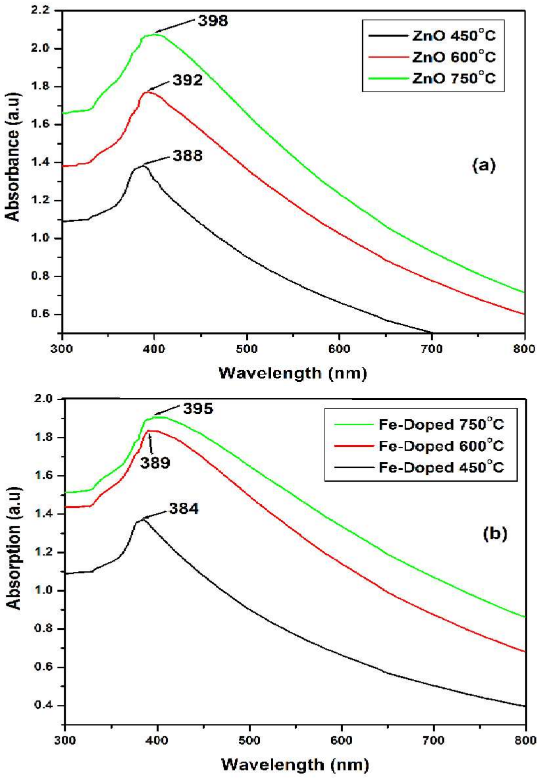

Fig. 6. UV-Vis absorption spectra of (a) pure ZnO (b) $Zn_{0.97}Fe_{0.03}O$ nanoparticles calcined at 450 °C, 600 °C and 750 °C.

localized d electron and band electrons of doped transition metal ions substituting the vacancy of cation. The observed increase in value of Eg with transition metal ion doping could be mainly due to Fe incorporation at substitutional or/and interstitial sites of wurtzite structure of ZnO.

Table 4. Optical parameters of pure ZnO nanoparticles calcined at 450 °C, 600 °C and 750 °C.

Calcination temperature [°C]	Absorption wavelength λ [nm]	Band gap energy (Eg = hc/λ) [eV]
450	388	3.20
600	392	3.17
750	398	3.12

3.4. Vibrating sample magnetometer (VSM) analysis

The room temperature M-H curves of the $Zn_{0.97}Fe_{0.03}O$ nanoparticles calcined at different temperatures in the magnetic field ranging from 0 kOe to ±20 kOe, obtained from VSM measurements are shown in Fig. 7. Magnetic parameters of all samples are summarized in Table 6. Fig. 7a and Fig. 7b show M-H curves for Fe-doped sample calcined at 450 °C, 600 °C and 750 °C. From Fig. 7a, it can be observed that the sample calcined at 450 °C has very low coercivity and remanence whereas its magnetization saturation is high. On the other hand, it is observed from Fig. 7b that with an increase in calcination temperature, magnetic saturation decreases whereas both coercivity and remanence of Fe-doped sample increase. The magnitude of thermal vibrations of atoms increases with the increase in temperature. The increase in thermal atomic motions neutralizes the coupling forces between the adjacent atomic dipole moments and it causes misalignment of some dipoles, irrespectively of external field. This results in a decrease in magnetic saturation.

Table 5. Optical parameters of $Zn_{0.97}Fe_{0.03}O$ nanoparticles calcined at 450 °C, 600 °C and 750 °C.

Calcination temperature [°C]	Absorption wavelength λ [nm]	Band gap energy (Eg = hv/λ) [eV]
450	384	3.23
600	389	3.19
750	395	3.15

So far, several reasons have been discussed to explain the origin of ferromagnetism and still this subject is controversial. One of the theories proposed that room temperature ferromagnetism is exhibited due to various intrinsic and extrinsic phenomena. Intrinsic phenomenon results from exchange interaction, and extrinsic phenomenon occurs due to formation of clusters or secondary phases of dopant semiconductor atoms [26].

In our study, the XRD and EDS results showed that dopant ions are successfully incorporated in the Zn wurtzite lattice without formation of any secondary phases and metallic clusters. However, there is a possibility of existence of secondary phases in the samples although they were not identified in our case. Therefore, let us consider all impurity phases that might be present

Table 6. Magnetic properties of $Zn_{0.97}Fe_{0.03}O$ nanoparticles.

$Zn_{0.97}Fe_{0.03}O$ [°C]	Coercivity Hc (Oe)	Remanent magnetization Mr [emu/g]	Magnetization saturation Ms [emu/g]
450	15 Oe	3.05×10^{-4}	0.234
600	42 Oe	3.75×10^{-4}	0.027
750	363 Oe	16.9×10^{-4}	0.006

in the samples and discuss about their ferromagnetic properties. Possible Fe-based oxides that might be present in Fe-doped samples are FeO and Fe_2O_3, Fe_3O_4 and $ZnFe_2O_4$. Secondary phases, such as FeO and Fe_2O_3 are anti-ferromagnetic at Neel temperature of 198 K and 963 K, respectively [27, 28]. Similarly, $ZnFe_2O_4$ phase is anti-ferromagnetic and can be excluded as the origin of ferromagnetism in our samples. In contrast to this, Fe_3O_4 phase is ferromagnetic but at Curie temperature of approximately 858 K [29]. Therefore, it is reasonable to conclude that the presence of ferromagnetic behavior in our samples is due to intrinsic coupling between the atoms of doped materials but not due to the presence of metallic clusters or secondary phases.

However, there are certain studies which claim that ferromagnetic behavior in transition metal-doped ZnO is correlated with defects such as oxygen or zinc vacancies [30–32]. Further, in some studies, the correlation between intrinsic defects such as oxygen or Zn vacancies and magnetism is also discussed [33, 34]. Karmakar et al. [35] investigated the origin of ferromagnetism in Fe-doped ZnO using ESR and Mössbauer spectroscopy. The analysis revealed that the Fe ions are present in both Fe^{2+} and Fe^{3+} valence states.

The presence of uncoupled Fe^{3+} ions is possibly due to hole doping in the system, which is caused by cation (i.e. Zn) vacancies. Therefore, once again it is concluded that the ferromagnetism observed in our $Zn_{0.97}Fe_{0.03}O$ sample was due to the presence of Fe atoms in the form of Fe^{2+} and Fe^{3+} ions.

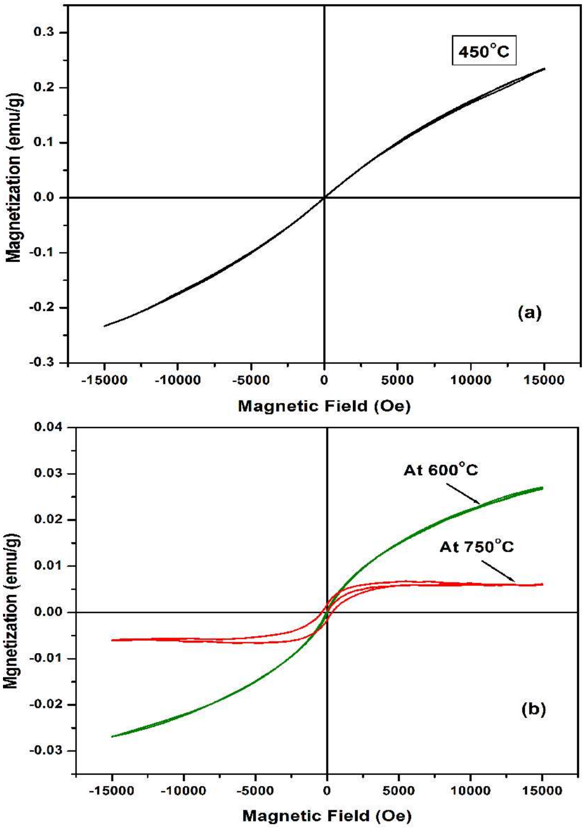

Fig. 7. Room temperature M-H curve of $Zn_{0.97}Fe_{0.03}O$ nanoparticles calcined at (a) 450 °C, (b) 600 °C and 750 °C calcination temperature.

4. Conclusions

In our investigations, pure ZnO and Fe-doped ZnO nanoparticles calcined at 450 °C, 600 °C and 750 °C were successfully synthesized through simple co-precipitation technique. X-ray diffraction pattern analysis confirms the formation of hexagonal wurtzite structure of ZnO with no evidence of any phase segregation for all samples. XRD patterns also reveal that the quality of crystal formation and particle size is sensitive to the calcination temperature. Both crystallinity and particle size increase with an increase in calcination temperature. UV-absorption spectrum shows red shift in wavelength for the sample calcined at higher temperature as compared to the sample calcined at lower temperature. Therefore, the band gap energy decreases with an increase in calcination temperature. Further, M-H curves for Fe-doped ZnO diluted magnetic semiconductor shows that room temperature ferromagnetism is also very much susceptible to calcination temperature. At lower temperature (450 °C), the sample is feebly ferromagnetic with very low coercivity and remanence but high magnetic saturation. On the other hand, at 600 °C and 750 °C the sample shows proper S-shaped M-H curves which confirms its ferromagnetic behavior. Also, both coercivity and remanence increase with calcination temperature but magnetic saturation decreases as compared to the sample calcined at 450 °C.

Therefore, we conclude that the structural, optical and magnetic properties of pure and doped ZnO nanoparticles can be controlled by varying calcination temperature.

References

[1] LING Z., LEOCH C., FREER R., *J. Eur. Ceram. Soc.*, 21 (2001), 1977.

[2] HSU C.Y., KU T.F., HUANG Y.M., *J. Eur. Ceram. Soc.*, 28 (2008), 3065.

[3] KUMAR S.S., VENKATESWARLU P., RAO V.R., RAO G.N., *Int. Nano Lett.*, 3 (30) (2013), 2345.

[4] WOLF S.A., AWSCHALOM D.D., BUHRMAN R.A., DAUGHTON J.M., MOLNAR S.V., ROUKES M.L., CHICHEL-KANOVA A.Y., TREGER D.M., *Science*, 294 (2001), 1488.

[5] OHNO H., *Science*, 281 (1998), 951.

[6] PRINZ G.A., *Science*, 282 (1998), 1660.

[7] GHOSH S., MANDAL K., *J. Magn. Magn. Mater.*, 322 (2010), 1979.

[8] WESSELINOWA J.M., APOSTO A.T., *J. Appl. Phys.*, 107 (2010), 053917.

[9] KARMAKAR D., MANDAL S.K., KADAM R.M., PAULOSE P.L., RAJARAJAN A.K., NATH T.K., DAS A.K., DASGUPTA I., DAS G.P., *Phys. Rev. B*, 75 (2007), 144404.

[10] MANDAL S.K., DAS A.K., NATH T.K., KARMAKAR D., SATPATI B., *J. Appl. Phys.*, 100 (2006), 104315.

[11] MARTINEZ B., SANDIUMENGE F., BALCELLS L., ARBIOL J., SIBIEUDE F., MONTY C., *Phys. Rev. B*, 72 (2005), 165202.

[12] DUAN L.B., RAO G.H., YU J., WANG Y.C., *Solid State Commun.*, 145 (2008), 525.

[13] LUO J., LIANG J.K., LIU Q.L., LIU F.S., ZHANG Y., SUN B.J., RAO G.H., *J. Appl. Phys.*, 97 (2005), 086106.

[14] WANG J.B., HUANG G.J., ZHONG X.L., SUN L.Z., ZHOU Y.C., LIU E.H., *Appl. Phys. Lett.*, 88 (2006), 252502.

[15] JAYAKUMAR O.D., GOPALAKRISHNAN I.K., SUDAKAR C., KADAM R.M., KULSHRESHTHA S.K., *J. Cryst. Growth*, 300 (2007), 358.

[16] BHUIYAN M.R.A., RAHMAN M.K., *Int. J. Precis. Eng. Man.*, 1 (2014), 10.

[17] VIJAYAPRASATH G., MURUGAN R., RAVI G., *Int. J. ChemTech Res.*, 6 (2014), 3385.

[18] KHATOON S., AHMAD T., *Mater. Sci. Eng. B-Adv.*, 2 (2012), 325.

[19] JADHAV J., PATANGE M., BISWAS S., *Carbon-Sci. Tech.*, 5 (2013), 269.

[20] VETHANATHAN S.J.K., PERUMAL S., SUNDAR S.M., KOILPILLAI D.P., KARPAGAVALLI S., SUGANTHI A., *Int. J. Adv. Sc. Tech. Res.*, 6 (2013), 856.

[21] FAHEEM A., SHALENDRA K., NISHATI A., ANWAR M.S., HEO S.N., KOO B.H., *Acta Mater.*, 60 (2012), 5190.

[22] LINHUA X., XIANGYIN L., *J. Cryst. Growth*, 312 (2010), 851.

[23] WANG C., CHEN Z., HE Y., LI L., ZHANG D., *Appl. Surf. Sci.*, 255 (2009), 6881.

[24] AYDIN C., ABD EL-SADEK M.S., ZHENG K., YAHIA I.S., YAKUPHANOGLU F., *Opt. Laser Technol.*, 48 (2013), 447.

[25] MORALES A.E., MORA E.S., PAL U., *Rev. Mex. Fis.*, 53 (2007), 18.

[26] SHARMA V.K., VARMA G.D., *Adv. Mat. Lett.*, 3 (2012), 126.

[27] WANG D., CHEN Z.Q., WANG D.D., CONG J., CAO C.Y., TANG Z., HUANG L.R., *J. Magn. Magn. Mater.*, 322 (2010), 3642.

[28] SANTOS D.A.A., MACEDO M.A., *Physica B*, 407 (2012), 3229.

[29] LIN F., JIANG D.M., MA X.M., *Physics B*, 405 (2010), 1466.

[30] CONG C.J., HONG J.H., ZHANG K.L., *Mater. Chem. Phys.*, 113 (2009), 435.

[31] XIONG Z., LIU X.C., ZHUO S.Y., YANG J.H., SHI E.W., YAN W.S., *Appl. Phys. Lett.*, 99 (2011), 052513.

[32] RAMACHANDRAN S., NARAYAN J., PRATER J.T., *Appl. Phys. Lett.*, 88 2006, 242503.

[33] BAPPADITYA P., GIRI P.K., *J. Nanosci. Nanotechno.*, 11 (2011), 1.

[34] SANTARA B., GIRI P.K., DHARA S., IMAKITA K., FUJII M., *J. Phys. D Appl. Phys.*, 47 (2014), 235304.

[35] KARMAKAR D., MANDAL S.K., KADAM R.M., PAULOSE P.L., RAJARAJAN A.K., NATH T.K., DAS A.K., DASGUPTA I., DAS G.P., *Phys. Rev. B.*, 75 (2007), 144404.

Received 2015-12-05
Accepted 2016-04-28